SENSOR LETTERS
Vol. 9, 670–674, 2011

Preparation and Humidity Sensitivity of Multi-Layered Zirconia Thin Films by Sol–Gel Method

Meiying Su and Jing Wang*

School of Electronic Science and Technology, Dalian University of Technology, Dalian 116023, P. R. China

(Received: 9 July 2010. Accepted: 11 November 2010)

Multi-layered zirconia (ZrO_2) thin film on the Pt/Ti/SiO_2/Si substrate has been prepared as humidity sensing material by sol–gel method. Annealing temperature was 450 °C. A TiO_2 thin film was added in between ZrO_2 film and the substrate for improving the adhesion. The films were characterized by using X-ray diffraction (XRD), atomic force microscope (AFM) and Fourier-transform infrared (FT-IR) spectra. The impedance of the humidity sensor changes about four orders of magnitude within the relative humidity (RH) range of 11–98%, indicating a good sensitivity. The response time of the sensor was about 5 s. The humidity sensing mechanism was discussed by means of the complex impedance curves and an equivalent circuit of the sensor.

Keywords: Humidity Sensor, Zirconia Thin Film, Sol–Gel, Multi-Layered.

1. INTRODUCTION

Many metal oxides were used as humidity sensing materials, such as ZnO,[1] TiO_2,[2] Al_2O_3[3] and SnO_2.[4] Zirconia (ZrO_2) with advantageous physical and chemical prosperities in "stabilized" state is applied as ceramic sensing material for gas sensor,[5–7] biosensor[8] and ultra-high-temperature fiber-optic sensors[9] and humidity sensors.[10, 11] To date, considerable researches were devoted to synthesize and characterize ZrO_2, and various methods have been conducted to fabricate ZrO_2 nano-particles and films.[12, 13]

In this paper, multi-layered ZrO_2 thin films were synthesized by sol–gel method. The humidity sensing properties of multi-layered ZrO_2 thin films were investigated and the humidity sensing mechanism was discussed by means of the complex impedance curves and an equivalent circuit of the sensor.

2. EXPERIMENTAL PROCEDURE

2.1. Multi-Layered Thin Films Fabrication

The ZrO_2 sol was prepared by mixing 3.22 g zirconium oxychloride ($ZrClO_2 \cdot 8H_2O$) and 50 ml ethanol, maintained the sol at 30 °C for 3 days. The TiO_2 sol was made by the following procedure: 8.5 ml of $Ti(OBu^n)_4$ was dissolved into 36 ml ethanol under vigorous agitation for 30 min, and then the mixture of 2 ml deionized water and 3 ml triethanolamine was added into the former solution. After agitated the solution for 2 hours, a yellow transparent viscous TiO_2 sol was obtained.

The TiO_2 precursor sol were placed on the Pt/Ti/SiO_2/Si substrate and spun at 3000 rpm for 30 s to form wet thin film, and then annealed at 450 °C. The thickness of TiO_2 film is 250 nm. The ZrO_2 films were prepared by the way as same as TiO_2 film. The thickness of the single layer ZrO_2 film is about 50 nm. After coated three times, the ZrO_2 films as one group annealed together at 450 °C formed the three-layered structure with total thickness of 150 nm films. The coating and annealing processes for ZrO_2 films were repeated twice to get 300 nm films, three times for 450 nm films. TiO_2 thin film was deposited directly on the substrates and annealed before the multi-layered ZrO_2 thin films were coated and annealed in order to avoid ZrO_2 cracks on platinum (Pt).

2.2. Material Characterization

The structures of ZrO_2 films were determined from conventional XRD (XRD-6000, Shimadzu, Japan). The morphology, roughness and grain size of the ZrO_2 thin films were investigated by using an AFM (CSPM5000, Benyuan, China). The FT-IR spectra of precursor sol and precursor thin films heated at different temperature (350, 450, 600 °C) were also performed by using a FT-IR

*Corresponding author; E-mail: wangjing@dlut.edu.cn

 1546-198X/2011/9/670/005 doi:10.1166/sl.2011.1588

spectrometer (EQUINOX55, Bruker, Germany), using KBr discs and recorded in the range 4000–400 cm^{-1}.

2.3. Sensor Measurement

Some electric parameters of the humidity sensor, such as impedance (Z), resistance (R), and dielectric loss (D) were measured at different relative humidities and frequencies by using an LCR intelligent test meter (Shanghai, China). The voltage applied in testing process was a.c. 1 V, and the frequency varied from 20 Hz to 100 kHz. The sensor was successively put into several chambers with different relative humidity levels at temperature about 20 °C. The different RH was obtained with saturated aqueous solutions of salts.

3. RESULTS AND DISCUSSION

3.1. Films Characterization

Figure 1 shows the XRD patterns of the zirconia thin films annealed at various temperatures. When the annealing temperature below 400 °C, zirconia film is an amorphous state, and as the annealing temperature increased, crystallization occurs and fine crystal cores are formed. Comparing the X-ray diffraction pattern with the powder diffraction file (PDF-ICSD), the main peak positions and intensities under 550 °C were close similar to the tetragonal phase (t-ZrO_2). At 600 °C monoclinic phase zirconia (m-ZrO_2) appears.

Figure 2 shows the IR spectra of the nanocrystal ZrO_2 gel powders annealed at 350 °C (curve (a)), 450 °C (b), and 600 °C (c), respectively. The Zr–O–Zr bending lines are observed in the region from 450∼800 cm^{-1}.[14, 15] During sintering, the Zr-O–Zr bonding peaks in tetragonal of ZrO_2 appear at around 460 cm^{-1} (curve (a)) and increase strongly with increasing annealing temperature (curve (b)),

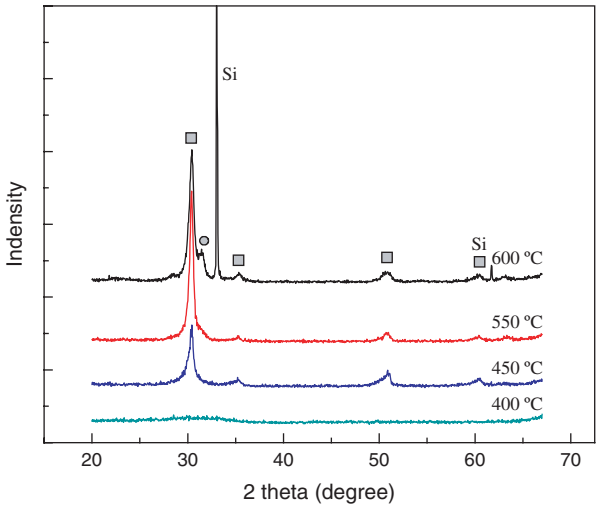

Fig. 1. XRD patterns of ZrO_2 thin film annealed at 400, 450, 550 and 600 °C (■ t-ZrO_2 • m-ZrO_2).

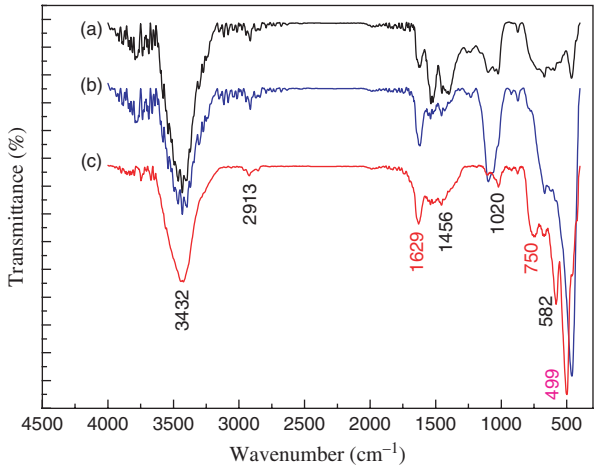

Fig. 2. FT-IR spectra of ZrO_2 gel powders annealed at (a) 350 °C, (b) 450 °C, (c) 600 °C.

and then become weak and have a little shift to high wavenumber after annealed at 600 °C. Meanwhile, the sharp bands at 582 cm^{-1} and 1020 cm^{-1} appear, which can be attributed to the characteristic band of monoclinic zirconia. The FT-IR spectra are in nice agreement with the XRD patterns of ZrO_2 thin film annealed at the correspondent temperature. These spectra also exhibit O–H stretching vibration around 3432 cm^{-1}, O–H bending vibration in the zirconium alkoxide, and C–H stretching vibration at 2913 cm^{-1}. These bonds indicate a certain amount of unhydrolyzed chelating segments and a small amount of solvent residues.[12, 15]

The morphology and roughness of the sample is characterized by AFM. Figure 3 shows AFM image of ZrO_2 thin film. The roughness and the average grain size of the ZrO_2 thin film are 2.29 and 25.5 nm, respectively.

3.2. Humidity Sensing Properties

Figure 4 gives the impedance versus relative humidity of the sensors with 150 nm thickness ZrO_2 thin films

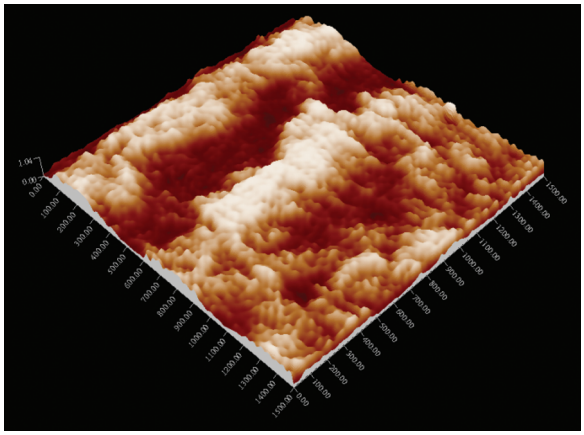

Fig. 3. AFM image of ZrO_2 thin film.

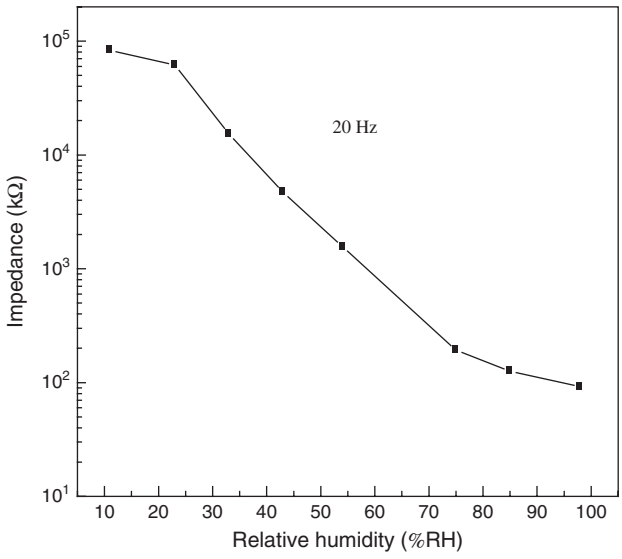

Fig. 4. Impedance versus relative humidity of 150 nm thickness ZrO_2 thin films at 20 Hz.

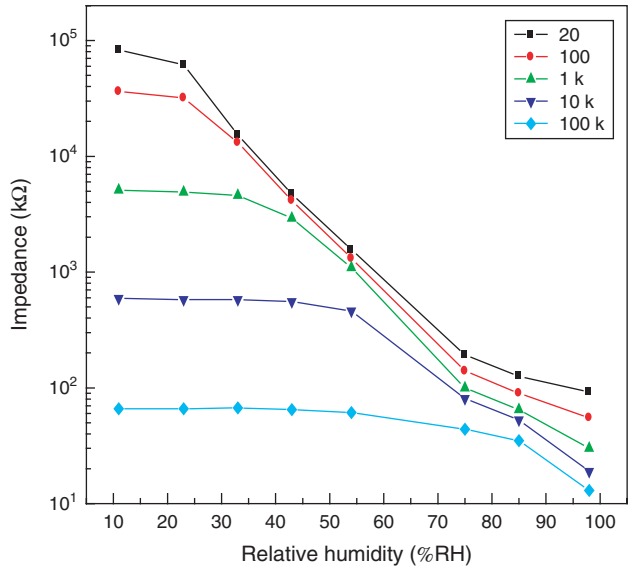

Fig. 5. Impedance versus relative humidity at different frequencies for 150 nm thickness ZrO_2 thin films.

at 20 Hz. The impedance of the sensors changed from 10^5 kΩ to 10^2 kΩ within the relative humidity varying from 11% to 98%, indicating a good sensitivity. The sensors with different thickness ZrO_2 films (150 nm, 300 nm, 450 nm) were also fabricated in this work. By comparison, the sensor with 150 nm thickness ZrO_2 films exhibited the better humidity sensing properties than the others, such as the range of measured humidity, linearity and so forth. This phenomenon was due to the dense surface, the thicker the films were, the harder for water molecules to penetrate. Secondly, during the films fabrication process, every three layer ZrO_2 films as one group were annealed at the same time, resulting in barriers between groups, so it is harder for water molecules to go through the barriers.

Figure 5 gives the impedance versus RH at different frequencies for 150 nm thickness ZrO_2 thin films. The linearity and sensitivity of the sensor are good for the lower frequencies, 20 Hz and 100 Hz. As the frequency increasing, the humidity sensing characterization of the sensor became weak.

The response and recover times are important parameters for evaluating the performance of a humidity sensor. Response time in the case of adsorption or recovery time in the case of desorption is defined as the time taken by the sensor to achieve 90% variable quantity. Figure 6 gives the response and the recovery processes between 22%RH and 98%RH. It can be seen that the response time was about 5 s. The recovery time was over 300 s.

3.3. Complex Impedance Analysis

To explain the humidity sensing mechanism of the sensor, an equivalent circuit was built on the ground of complex impedance diagrams. Complex impedance diagrams under different relative humidities were drawn, as shown in Figure 7. Within the frequency range of 10–10^5 Hz, the complex impedance diagram was like half semicircle when RH is low. As RH increased, the semicircle was completed and smaller, and a new spur denoted as the beginning of another semicircle appeared and became longer. As reported in paper,[16] two semicircle-like curves in Figure 7 was attributed to electric response at crystal boundary and electrode interface influenced by humidity significantly. We built an equivalent circuit of resistor (R) in parallel with constant phase element (CPE) as shown in Figure 8. Where R1, CPE1, R2, CPE2 represented the grain boundary resistance, grain boundary "non-Debye" capacitance, electrode interface resistance, and electrode interface "non-Debye" capacitance, respectively.

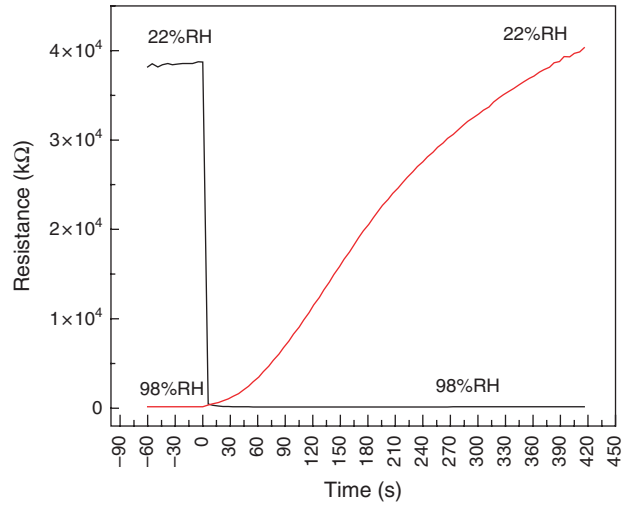

Fig. 6. Response and recovery curves of 150 nm thickness ZrO_2 thin films at 20 Hz.

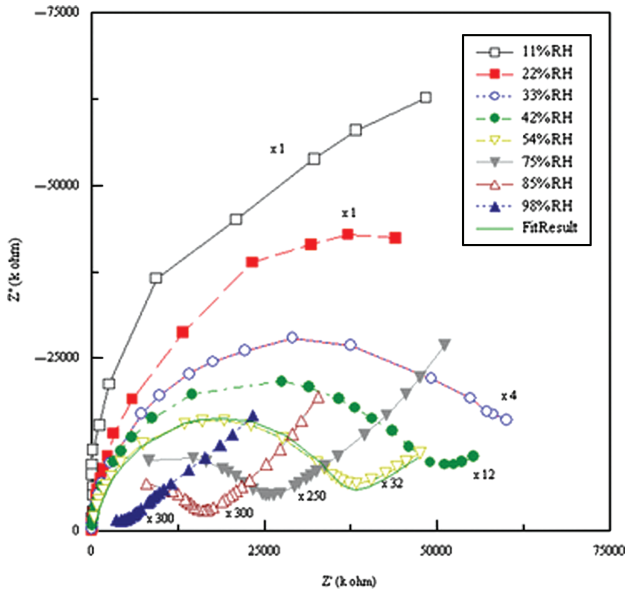

Fig. 7. Complex impedance diagrams of 150 nm thickness zirconia thin films humidity sensor at 20 °C. The solid line is the complex impedance fitting plots at 54%RH based on the equivalent circuit proposed in Figure 8. The circuit elements values were $R1 = 1082$ kΩ, CPE1-A = 7.16E-8, CPE1-$\alpha = 0.915$, $R2 = 1313$ kΩ, CPE2-A = 5.9E-5 and CPE2-$\alpha = 0.63$.

"Resistor" in the circuit represents conduction process and "CPE" represents complicated polarization process. A CPE is a simple distributed element that often used in a model in place of a capacitor to take account diffusion and interface phenomena. Impedance function of a CPE can be expressed as follows:[17]

$$Z_{\mathrm{CPE}} = \frac{1}{A(j\omega)^{\alpha}} \tag{1}$$

Here, A is the impedance modulus, j is square root of -1, ω is angle frequency, and α satisfies $-1 \leq \alpha \leq 1$. In the case of $\alpha = 1$, the CPE acts like a capacitor with capacitance equal to A. The CPE also can behave as resistor or inductance when $\alpha = 0$ or -1, respectively.

In the present paper, a.c. measurement data coming from 54%RH were fitted with the equivalent circuit using the software Zview 3.0 as shown in Figure 7. The solid line in the figure was fitting data, and the marks were raw data based on the equivalent circuit as mentioned above.

It is well known from water adsorption theory that chemisorption takes place at a few hundred centigrade due to its high adsorption enthalpy, and physisorption commences at lower temperature (blow 100 °C) due to a lower adsorption enthalpy,[17] so water chemi- sorption on ZrO_2 active sites had been done in the fabrication process of the sensor. Once the chemisorbed layer formed, it is hard affected by exposure to humidity, so the variation of electrical signal with humidity in the sensor is largely due to the amount of physisorbed water.

Fig. 8. Equivalent circuit of the 150 nm thickness ZrO_2 thin films humidity sensor.

The amount of physisorbed water depends on the magnitude of the relative humidity. At low relative humidity level, little water molecules were absorbed physically to form a discrete water layer on top of the chemisorbed one where the Zr–OH bondings were formed. When a physisorbed water molecule attached to two adjacent Zr–OH components, the defects including hydronium ions H_3O^+ and hydroxyl group OH^- were generated, resulting in the proton hopping. Simultaneously electrons from the sensing material also contributed to electrical conduction, compensating for the weak continuity of proton hopping conduction caused by the low coverage of water. As RH increases, more than one physisorbed water layer attached on the chemisorbed one, proton transfer mechanism dominated the conduction including the motion of hydronium and the hopping of a proton from a hydronium to a water molecule. When physisorbed water was abundant, a H_3O^+ is hydrated, $H_3O^+ \rightarrow H_2O + H^+$, H^+ as the mainly charge carrier transferred within the continuous water film, at the same time, water as electrolyte was also responsible for the electrical conduction.

4. CONCLUSIONS

Multi-layered nanometer zirconia thin films deposited on silicon substrate were prepared by sol–gel method and the humidity sensing properties of the thin films with various thickness were investigated, including high sensitivity, good linearity, response and recovery behavior. By analyzing the complex impedance curves, an equivalent circuit of the sensor was erected with a serial circuit of resistor in parallel with CPE, in order to explain the humidity sensing mechanism.

Acknowledgments: The subject was supported by The National Natural Science Foundation of China (60474052, 90607002) and 973 Projects (2011CB302101 and 2011CB302105) for financial support.

References and Notes

1. W. P. Tai and J. H. Oh, *J. Mater. Sci.: Mater. Electron.* 13, 391 (**2002**).
2. Z. C. Wang, U. Helmersson, and P. O. Kall, *Thin Solid Films* 405, 50 (**2002**).
3. K. S. Shamala, L. C. S. Murthy, M. C. Radhakrishna, and K. N. Rao, *Sens. Actuators, A* 135, 552 (**2007**).
4. Q. Kuang, C. Lao, Z. L. Wang, Z. Xie, and L. Zheng, *J. Am. Chem. Soc.* 129, 6070 (**2007**).
5. N. Rajabbeigi, B. Elyassi, A. A. Khodadadi, S. Mohajerzadeh, Y. Mortazavi, and M. Sahimi, *Sens. Actuators, B* 108, 341 (**2005**).

6. J. C. Yang and P. K. Dutta, *Sens. Actuators, B* 136, 523 **(2009)**.
7. K. I. Shimizu, K. Kashiwagi, H. Nishiyama, S. Akimoto, S. Sugaya, H. Yokoi, and A. Satsuma, *Sens. Actuators, B* 130, 707 **(2008)**.
8. G. Zhao, J. J. Feng, J. J. Xu, and H. Y. Chen, *Electrochem. Commun.* 7, 724 **(2005)**.
9. L. Tong, *J. Cryst. Growth* 217, 281 **(2000)**.
10. K. P. Biju and M. K. Jain, *Sens. Actuators, B* 128, 407 **(2008)**.
11. J. Wang, M. Y. Su, J. Q. Qi, and L. Q. Chang, *Sens. Actuators, B* 139, 418 **(2009)**.
12. L. P. Liang, Y. Xu, D. Wu, and Y. Sun, *Mate. Chem. Phys.* 114, 252 **(2009)**.
13. S. Iwatsubo and K. Ishii, *Vacuum* 83, 579 **(2009)**.
14. Y. Yu, X. P. Wang, Y. Z. Cao, and X. F. Hu, *Appl. Surf. Sci.* 172, 260 **(2001)**.
15. W. S. Dong, F. Q. Lin, C. L. Liu, and M. Y. Li, *J. Colloid. Interf. Sci.* 333, 734 **(2009)**.
16. E. Barsoukov and J. R. Macdonald, In Impedance Spectroscopy Theory, edited by I. D. Raistrick, D. R. Franceschetti, and J. R. Macdonald, John Wiley and Sons, Inc., Hoboken, New Jersey **(2005)**, Chap. 2, pp. 27–128.
17. P. M. Faia, A. J. Ferreira, and C. S. Furtado, *Sens. Actuators, B* 140, 128 **(2009)**.